Received: 21 June 2019 | Revised: 12 May 2020 | Accepted: 19 May 2020

DOI: 10.1096/fj.201901321R

RESEARCH ARTICLE

THE FASEB JOURNAL

The importance of the ZBED6-IGF2 axis for metabolic regulation in mouse myoblast cells

Shady Younis[1] | **Rakan Naboulsi**[1] | **Xuan Wang**[2] | **Xiaofang Cao**[1] | **Mårten Larsson**[1] | **Ernest Sargsyan**[2] | **Peter Bergsten**[2] | **Nils Welsh**[2] | **Leif Andersson**[1,3,4]

[1]Science for Life Laboratory, Department of Medical Biochemistry and Microbiology, Uppsala University, Uppsala, Sweden

[2]Science for Life Laboratory, Department of Medical Cell Biology, Uppsala University, Uppsala, Sweden

[3]Department of Animal Breeding and Genetics, Swedish University of Agricultural Sciences, Uppsala, Sweden

[4]Department of Veterinary Integrative Biosciences, Texas A&M University, College Station, TX, USA

Correspondence
Leif Andersson, Science for Life Laboratory, Department of Medical Biochemistry and Microbiology, Uppsala University, Box 582, Uppsala SE-751 23, Sweden.
Email: leif.andersson@imbim.uu.se

Funding information
Knut och Alice Wallenbergs Stiftelse (Knut and Alice Wallenberg Foundation), Grant/Award Number: KAW Scholar; Swedish Research Council, Grant/Award Number: Rådsprofessur

Abstract

The transcription factor ZBED6 acts as a repressor of *Igf2* and affects directly or indirectly the transcriptional regulation of thousands of genes. Here, we use gene editing in mouse C2C12 myoblasts and show that ZBED6 regulates *Igf2* exclusively through its binding site 5′-GGCTCG-3′ in intron 1 of *Igf2*. Deletion of this motif ($Igf2^{\Delta GGCT}$) or complete ablation of *Zbed6* leads to ~20-fold upregulation of the IGF2 protein. Quantitative proteomics revealed an activation of Ras signaling pathway in both $Zbed6^{-/-}$ and $Igf2^{\Delta GGCT}$ myoblasts, and a significant enrichment of mitochondrial membrane proteins among proteins showing altered expression in $Zbed6^{-/-}$ myoblasts. Both $Zbed6^{-/-}$ and $Igf2^{\Delta GGCT}$ myoblasts showed a faster growth rate and developed myotube hypertrophy. These cells exhibited an increased O_2 consumption rate, due to IGF2 upregulation. Transcriptome analysis revealed ~30% overlap between differentially expressed genes in $Zbed6^{-/-}$ and $Igf2^{\Delta GGCT}$ myotubes, with an enrichment of upregulated genes involved in muscle development. In contrast, ZBED6-overexpression in myoblasts led to cell apoptosis, cell cycle arrest, reduced mitochondrial activities, and ceased myoblast differentiation. The similarities in growth and differentiation phenotypes observed in $Zbed6^{-/-}$ and $Igf2^{\Delta GGCT}$ myoblasts demonstrates that ZBED6 affects mitochondrial activity and myogenesis largely through its regulation of IGF2 expression. This study adds new insights how the ZBED6-*Igf2* axis affects muscle metabolism.

KEYWORDS

IGF2, mitochondria, myogenesis and gene editing, ZBED6

Abbreviations: BCA, bicinchoninic acid; CPM, counts per million; DE, differentially expressed; ECAR, extracellular acidification rate; ECM, extra cellular matrix; FA, formic acid; FDR, false discovery rate; G0/G1 phase, growth phase in cell cycle; GO, gene ontology; gRNA, guideRNA; HCM, hypertrophic cardiomyopathy; Igf2ΔGGCT, a four-nucleotide deletion (GGCT) of the ZBED6-binding motif in Igf2; Igf2Δ120bp, a 120 bp deletion in Igf2; logCPM, log counts per million; logFC, log fold change; MyHC, Myosin heavy chain; OCR, oxygen consumption rate; S-phase, synthesis phase in cell cycle; TMM, trimmed mean of M-values; ZBED6-GFP, GFP-tagged ZBED6; ZBED6-OE, ZBED6 overexpression.

1 | INTRODUCTION

The ZBED6 transcription factor is unique to placental mammals and has evolved from a domesticated DNA transposon located in the first intron of *ZC3H11A*, a zinc-finger protein with RNA-binding capacity.[1,2] ZBED6 was identified as a repressor of insulin-like growth factor 2 (*IGF2)* expression following the identification of a mutation in *IGF2* intron 3 in domestic pigs.[1,3] This mutation disrupts a ZBED6 binding site and leads to a three-fold increase in the *IGF2* mRNA expression in pig skeletal muscle, which in turn results in increased muscle mass and reduced subcutaneous fat deposition. We have previously reported that ZBED6 has thousands of putative binding sites in human and mouse genomes, with a strong enrichment in the vicinity of transcription start sites (TSS) of genes involved in development and transcriptional regulation.[1,4-6] However, it is still unknown which of these genes, besides *Igf2*, are true functional targets of ZBED6. Silencing of *Zbed6* expression in mouse C2C12 myoblasts using small interfering RNA (siRNA) resulted in differential expression of about 700 genes, including a three-fold upregulation of *Igf2* mRNA.[4] IGF2 is an essential growth factor in skeletal muscle development and has a role in the initiation of myoblast differentiation.[7] Recently, we have developed *Zbed6*$^{-/-}$ and *Igf2* knock-in mice, the latter carrying the pig mutation at the ZBED6 binding site. These mice exhibited increased body weight and skeletal muscle growth.[8] However, the molecular mechanism how ZBED6 affects muscle growth has not been fully investigated. Particularly, the interaction between ZBED6 and *Igf2* during myogenesis, and to which extent phenotypic changes associated with altered ZBED6 expression is mediated through its interaction with the *IGF2* locus has hitherto not been studied.

In recent years, the genome editing technique based on the microbial Clustered Regularly Interspaced Short Palindromic Repeats (CRISPR) and CRISPR-associated protein 9 (Cas9) nucleases, has become the most efficient method to knockout a gene of interest or manipulate a specific site in mammalian cells.[9,10] We employed this technology to explore the significance of ZBED6-*Igf2* interaction in the mouse myoblast C2C12 cell line that has the ability to differentiate and form myotubes.[11] In the present study, we generated two models of engineered C2C12 cells, a *Zbed6* knockout and a deletion of the ZBED6 binding site in an *Igf2* intron. The genetically modified C2C12 cells were induced to differentiate, followed by whole transcriptome analysis, mass spectrometry (MS)-based quantitative proteomics and detailed functional characterizations of myoblast proliferation and myotube formation.

2 | MATERIALS AND METHODS

2.1 | Cell culture

Mouse myoblast C2C12 cells were obtained from ATCC (CRL-1772), and it is a subclone of the previously established mouse myoblast cell line.[11] The cells were maintained in Dulbecco's Modified Eagle Medium (DMEM) with 2 mM L-glutamine, 1 mM sodium pyruvate, and 4.5 g/L of glucose (ATCC 30-2001), supplemented with 10% (v/v) heat-inactivated fetal bovine serum (FBS) and penicillin (0.2 U/mL)/streptomycin (0.2 μg/mL)/L-glutamine (0.2 μg/mL) (Gibco) at 37°C in a 5% CO_2 humidified atmosphere. Differentiation was induced by replacing FBS with 2% horse serum (Gibco). The differentiation medium was changed every 48 hours. The differentiated myotubes were collected by adding 0.05% Trypsin-EDTA (Gibco) for 1 minute at 37°C, which was sufficient to detach the mature myotubes from the plate.

2.2 | Genome editing

The coding sequence of *Zbed6* and its binding site in *Igf2* were targeted in C2C12 cells using CRISPR/Cas9 tools. Two specific guide RNAs (gRNA) for *Zbed6* and one for *Igf2* were designed using the CRISPRdirect tools.[12] The gRNAs sequences were cloned into the Cas9 expressing plasmid pSpCas9(BB)-2A-GFP (PX458), (Addgene plasmid #48138) and co-transfected with linear hygromycin marker (Clontech) into C2C12 cells at passage number 5. Wild-type (WT) cells were transfected with empty pSpCas9(BB)-2A-GFP plasmid and linear hygromycin. Transfected cells were kept under selective medium for 2 weeks. Single-cell clones were screened for a 2.5 kb deletion in *Zbed6* using primers flanking the targeted site (Figure 1A). The *Igf2* targeted clones were screened using primers flanking the targeted site, followed by Sanger sequencing of individual clones.

2.3 | Immunofluorescence staining

Cells were cultured in an 8-well slide chamber (BD Falcon) overnight to around 60-70% confluence. The cells were washed with PBS and fixed with 4% (v/v) paraformaldehyde for 10 minutes at room temperature. The fixed cells were permeabilized with 0.25% (v/v) Triton X-100 and then blocked for non-specific binding with 2% (w/v) BSA in PBS. The primary antibodies for myogenin and myosin heavy chain (Santa Cruz Biotechnology) were diluted 1:500 in PBS containing 1% (w/v) BSA and incubated with the cells overnight. Cells were washed three times with PBS and then incubated with Alexa Flour-labeled secondary antibodies. DAPI was used as counter staining. Slides were analyzed using a confocal microscope (Zeiss LSM 700).

2.4 | Real-time quantitative PCR

Total RNA was extracted from cells using the RNeasy Mini kit (Qiagen), including the DNase I treatment. The

High Capacity cDNA Reverse Transcription Kit (Applied Biosystems) was used to generate cDNA from the extracted RNA. Quantitative PCR (qPCR) analysis was performed using ABI MicroAmp Optical 384-well Reaction plates on an ABI 7900 real-time PCR instrument (Applied Biosystems). The qPCR was performed using TaqMan Gene Expression

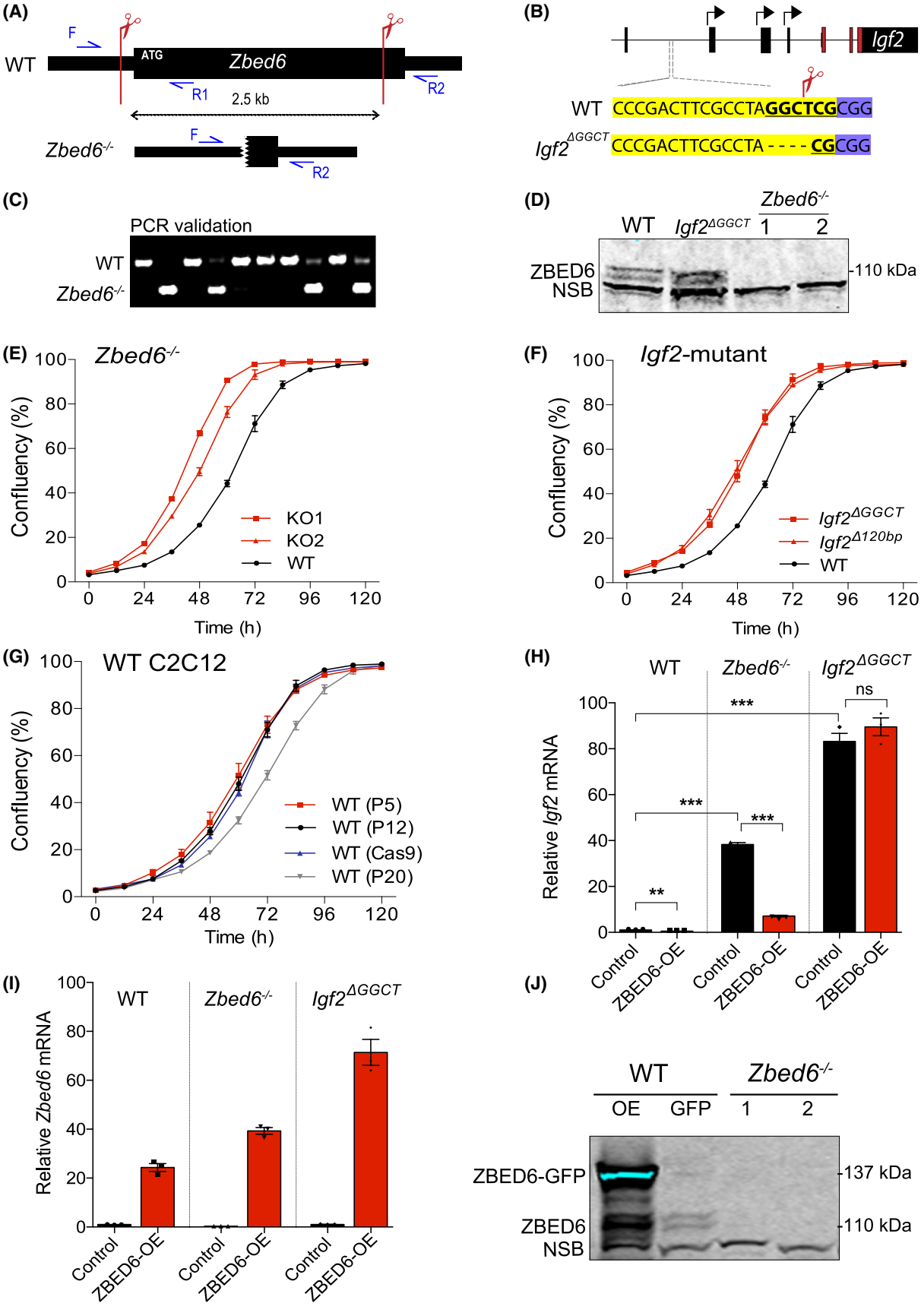

FIGURE 1 Knockout of *Zbed6* or its binding site in *Igf2* alter the growth of myoblasts. A, Schematic description of Zbed6 targeting using CRISPR/Cas9. Red scissors indicate the targeted sites of *Zbed6* using two gRNAs. Blue arrows indicate the location of the PCR primers that were used for genotyping of the KO clones. B, Schematic description of the targeted ZBED6 binding sequences in *Igf2* (bold). The scissor indicates the cleavage site using specific gRNA sequences (yellow) adjacent to the PAM sequences (blue). Black arrows indicate *Igf2* promoters, red boxes are the coding sequences of Igf2. C, PCR screening of *Zbed6* KO clones. D, Immunoblot validation of $Zbed6^{-/-}$ clones, the $Igf2^{\Delta GGCT}$ clone and WT cells, NSB: non-specific band. E, Real-time measurements of cell growth (mean ± SEM) of WT C2C12 cells (black) and $Zbed6^{-/-}$ clones (red) (n = 3). F, Cell growth of two *Igf2*-mutant clones (red) and WT cells (black). G, Cell growth measurement of WT C2C12 cells at different passages (P5, P12, and P20) and WT cells transfected with Cas9 reagents without gRNA (WT Cas9). H, Quantitative PCR analysis of the *Igf2* mRNA expression after transient expression of ZBED6-GFP in WT cells, $Zbed6^{-/-}$ and $Igf2^{\Delta GGCT}$ cells. I, Quantitative PCR analysis of the *Zbed6* mRNA expression and after transient expression of GFP (Control) or ZBED6-GFP (ZBED6-OE) constructs in myoblasts. J, Immunoblot validation of ZBED6-GFP overexpression in C2C12 cells. Graph shows the fold changes (mean ± SEM) compared to WT control cells. ns = non significant, $^{**}P < .01$, $^{***}P < .001$, Student's *t* test

Assays that consisted of forward and reverse primers with TaqMan minor groove binder (MGB) probe for each gene (*Zbed6*: Mm04178798_s1, *Igf2*: Mm00439564_m1, *18S*: Mm03928990_g1, Applied Biosystems); 18S and was used as housekeeping gene. For *Myog* and the validated differentially expressed (DE) genes, the forward and reverse primers (Table S6) were mixed with SYBR Green Gene Expression Master Mix (Applied Biosystems) in 10 µL of total reaction volume.

2.5 | Immunoblot analysis

Total protein lysates were prepared using RIPA lysis buffer containing protease inhibitors (Complete Ultra Tablets, Roche). Equal amounts of total lysates were separated by SDS-PAGE (4-15%, Bio-Rad) and transferred to PVDF membranes (Millipore). StartingBlock buffer (Thermo Scientific) was used to block the membrane before the primary anti-ZBED6 antibody (1:1000) was added.[5] Proteins were visualized and detected by the Odyssey system (LI-COR).

2.6 | Stable isotope labeling with amino acids in cell culture

C2C12 cells were cultured in Dulbecco's modified Eagle's medium (DMEM) for Stable Isotope Labeling with Amino acids in Cell culture (SILAC) (Thermo Fisher Scientific) supplemented with 10% dialyzed fetal bovine serum (FBS, MWCO 10 kDa; Thermo Fisher Scientific), 100 U/mL of penicillin (Thermo Fisher Scientific), 100 µg/mL of streptomycin (Thermo Fisher Scientific), 0.25 µg/mL of amphotericin B (Thermo Fisher Scientific) and light isotopic labels L-arginine-HCl and L-lysine-2 HCl or heavy isotopic labels $^{13}C_6$, $_{15}$N4 L-arginine-HCl (Arg-10) and $^{13}C_6$, $^{15}N_2$ L-lysine-2 HCl (Lys-8) (Thermo Fisher Scientific). Cells were kept in a humidified atmosphere with 5% CO_2 at 37°C. To avoid contamination of light amino acids, sub-culturing was performed using Cell dissociation buffer (Thermo Fisher Scientific) instead of trypsin. Isotopic incorporation was checked using a script in R as previously described[13] after approximately five cell divisions to confirm complete (>95%) labeling. Arginine-to-proline conversion was assessed by calculating the percentage of heavy proline (Pro-6) containing peptides among all identified peptides, and kept at <5%. Confluent (~80%) cells were washed five times with PBS, and incubated 12 hours in serum-free medium. Medium was collected, centrifuged and filtered through a 0.2 µm filter. Protein concentration was measured with a Coomassie (Bradford) assay kit (Thermo Fisher Scientific). Cells were harvested and lysates prepared using M-PER mammalian protein extraction reagent (Thermo Fisher Scientific), and protein concentration was measured using a bicinchoninic acid (BCA) protein assay kit (Thermo Fisher Scientific). Heavy and light cell lysates or media (40 µg each of cell lysate, 170 µg each of medium) were mixed 1:1. Mixed media were subsequently concentrated through spin columns with a cutoff of 3 kDa (Vivaspin, Sartorius). Mixed proteins were separated on a 4%-20% Mini-PROTEAN TGX precast gel (Bio-Rad, Hercules, CA). Each gel lane was cut into 10 separate pieces, and proteins were reduced in-gel with 10 mM DTT in 25 mM NH_4HCO_3, thereafter, alkylated with 55 mM iodoacetamide in 25 mM NH_4HCO_3, and finally digested with 17 ng/µL sequencing-grade trypsin (Promega) in 25 mM NH_4HCO_3 using a slightly modified in-gel digestion protocol.[14] The produced peptides were eluted from the gel pieces using 1% (v/v) formic acid (FA) in 60% (v/v) acetonitrile, dried down in a vacuum centrifuge (ThermoSavant SPD SpeedVac, Thermo Scientific), and finally dissolved in 1% (v/v) FA. The experiments were run in at least triplicate, of which at least one was reciprocal (reverse labeling).

2.7 | Liquid chromatography and mass spectrometry

Peptide samples were desalted using Stage Tips (Thermo Fisher Scientific) according to the manufacturer's protocol, and subsequently dissolved in 0.1% (v/v) FA. Samples were separated by RP-HPLC using a Thermo Scientific nLC-1000 with a two-column setup; an Acclaim PepMap 100

(2 cm × 75 µm, 3 µm particles, Thermo Fisher Scientific) pre-column was connected in front of an EASY-Spray PepMap RSLC C18 reversed phase column (50 cm × 75 µm, 2 µm particles, Thermo Fisher Scientific) heated to 35°C, running solvent A (H_2O and 0.1% (v/v) FA). A gradient of 2-40% solvent B (acetonitrile and 0.1% (v/v) FA) was run at 250 nL/min over a period of 3 hours. The eluted peptides were analyzed on a Thermo Scientific Orbitrap Fusion Tribrid mass spectrometer, operated at a Top Speed data-dependent acquisition scan mode, ion-transfer tube temperature of 275°C, and a spray voltage of 2.4 kV. Full scan MS spectra (m/z 400-2000) were acquired in profile mode at a resolution of 120 000 at m/z 200, and analyzed in the Orbitrap with an automatic gain control target of 2.0e5 and a maximum injection time of 100 ms Ions with an intensity above 5.0e3 were selected for collision-induced dissociation fragmentation in the linear ion trap at a collision energy of 30%. The linear ion trap automatic gain control target was set at 1.0e4 with a maximum injection time of 40 ms, and data were collected at centroid mode. Dynamic exclusion was set at 60 seconds after the first MS1 of the peptide. The system was controlled by Xcalibur software (version 3.0.63.3, Thermo Scientific). Instrument quality control was monitored using the Promega 6x5 LC-MS/MS Peptide Reference Mix (Promega) before and after each MS experiment run, and analyzed using PReMiS software (version 1.0.5.1, Promega).

2.8 | Mass spectrometric data analysis

Data analysis of raw files was performed using MaxQuant software (version 1.5.6.5) and the Andromeda search engine,[15,16] with cysteine carbamidomethylation as a static modification and Arg-10, Lys-8, methionine oxidation, and protein N-terminal acetylation as variable modifications. First search peptide MS1 Orbitrap tolerance was set to 20 ppm. Iontrap MS/MS tolerance was set to 0.5 Da. The re-quantify option was enabled to get ratios where only one isotope pattern was found. Match between runs was also enabled, to identify peptides where only MS1 data were available. Minimum label ratio count was set to 1, and the advanced ratio estimation option was enabled. Peak lists were searched against the UniProtKB/Swiss-Prot *Mus musculus* proteome database (UP000000589, version 2016-01-12) with a maximum of two trypsin miscleavages per peptide. The contaminants database of MaxQuant was also utilized. A decoy search was made against the reversed database, where the peptide and protein false discovery rates were both set to 1%. Only proteins identified with at least two peptides of at least seven amino acids in length were considered reliable. The peptide output from MaxQuant was filtered by removing reverse database hits, potential contaminants and proteins only identified by site (PTMs). Intensity values were first normalized using variance stabilization method, adjusted for batch effect and fitted to linear model.[17,18] The empirical Bayes moderated t-statistics and their associated *P*-values were used to calculate the significance of DE proteins.[19] The *P*-values were corrected for multiple testing using the Benjamini-Hochberg procedures.[20] The mass spectrometry proteomics data have been deposited to the ProteomeXchange Consortium via the PRIDE partner repository with the dataset identifiers PXD012757, PXD012758, PXD012769, and PXD012789.

2.9 | RNA sequencing

Myoblasts or the collected myotubes were washed in PBS and total RNA was extracted using the RNeasy Mini kit (QIAGEN). The RNA quality and integrity were measured with a RNA ScreenTape assay (TapeStation, Agilent Technologies). Strand-specific, 3′ end mRNA sequencing libraries were generated using QuantSeq 3′ mRNA-Seq Library Prep Kit (Lexogen) following the manufacturer's instructions. For each sample, 2 µg of total RNA were poly-A selected using oligo-dT beads to enrich for mRNA, and the RNA-seq libraries were amplified by 12 PCR cycles. The libraries were size-selected for an average insert size of 150 bp and sequenced as 50 bp paired-end reads using Illumina HiSeq. Sequence reads were mapped to the reference mouse genome (mm10) using STAR 2.5.1b with default parameters.[21] HTSeq-0.6.1 (Python Package)[22] was used to generate read counts and edgeR (Bioconductor package)[23] was used to identify (DE) genes using gene models for mm10 downloaded from UCSC (www.genome.ucsc.edu). The abundance of gene expression was calculated as counts per million (CPM) reads. Genes with less than one CPM in at least three samples were filtered out. The filtered libraries were normalized using the trimmed mean of M-values (TMM) normalization method.[24] *P*-values were corrected for multiple testing using the False Discovery Rate (FDR) approach. The DE genes were submitted to The Database for Annotation, Visualization and Integrated Discovery (DAVID, v6.8)[25] for gene ontology analysis. All expressed genes in C2C12 cells were used as background, and the Biological Process and KEGG pathway tables were used to identify enriched GO terms.

2.10 | Cell growth measurements

Wild-type cells at different passages (P5, P12, and P12), WT cells transfected with the Cas9 plasmid (WT-Cas9), two *Zbed6*$^{-/-}$ and two *Igf2*-mutant clones were seeded in 24-well plates (10 000 cells per well) in growth media, and

were cultured for 6 days with real-time measurement of cell density every 12 hour using an IncuCyte instrument (Essen Bioscience). The experiments were carried out using biological triplicates of each cell line.

2.11 | Cell viability assay

Cells were seeded in 24-well plates (30 000 cells/well) and let to attach. A day after, the cells were transfected with GFP (control) or ZBED6-GFP overexpressing constructs (ZBED6-OE). At 24 hours post transfection, the cells were incubated with growth media containing 10% (v/v) PrestoBlue (Invitrogen). The reduction of PrestoBlue reagent was measured on a Tecan Sunrise Plate Reader at four time points post incubation (10 minutes, 30 minutes, 2 hours, and 4 hours), with the following parameters: bottom-read fluorescence (excitation 560 nm, emission 590 nm).

2.12 | Cell cycle analysis

C2C12 cells transiently expressing ZBED6-GFP or GFP were analyzed for cell cycle profile using Click-iT EdU flow cytometry assay kit (Invitrogen) and FxCycleTM violet stain (Invitrogen) for total DNA staining. Cells were incubated with EdU for 2 hours according to the manufacturer's instructions before fixation and DNA staining. Cells were analyzed on an LSR Fortessa (BD Biosciences), and results were analyzed using the FACSDiva software (BD Biosciences).

2.13 | Cell apoptosis

C2C12 cells were harvested and fixed with 4% PFA (not permeabilized), and controls were fixed and permeabilized with Cytofix/Cytoperm solution (BD Biosciences) before staining with V450-Annexin-V (BDBiosciences) and/or DRAQ7 (Biostatus). Cells were stained with V450-Annexin-V and DRAQ7 according to the manufacturer's protocol. Cells were incubated for 15-30 minutes at RT in dark. Samples were analyzed on a BD LSRFortessa flow cytometer using the BD FACSDiva software. Viable cells were Annexin-V negative and DRAQ7 negative (AnnV-, PI-) staining, while cells in early apoptosis were Annexin-V positive and DRAQ7 negative. Cells in late-apoptosis/necrosis were Annexin-V positive and DRAQ7 positive.

2.14 | MitoTracker Red and JC-1 staining

C2C12 cells were stained for active mitochondria by 50nM MitoTracker Red FM (Invitrogen) for 30 minutes. After washing, the cells were either fixed for confocal imaging by a Zeiss 780 confocal microscope or directly examined for MitoTracker Red intensity using a FACSCalibur flow cytometer (BD Biosciences). Mitochondrial membrane potential of C2C12 cells was semiquantitatively determined by the fluorescent probe JC-1 (4 μM, 30 minutes incubation, Sigma-Aldrich). After careful washing, the cells were imaged by confocal microscope and the fluorescence of JC-1 aggregates at hyperpolarized membrane potential (585 nm) was quantified by Image J.

2.15 | Oxygen consumption and extracellular acidification rates

The oxygen consumption rate (OCR) and extracellular acidification rate (ECAR) were determined using the Extracellular Flux Analyzer XF^{e}96 (Seahorse Bioscience). Cells were cultured in 96-well plates (Seahorse Biosciences) in normal culture medium for 24-48 hours. After culture, assays were performed in XF assay medium (Seahorse Biosciences) set to pH 7.4 and supplemented with 25 mM glucose. OCR and ECAR were measured during the last 30 minutes of the 1 hour incubation in XF assay medium, which was followed by the injection of inhibitors of the electron transport chain, 5 μmol/L rotenone and 5 μmol/L antimycin A, to inhibit the mitochondrial respiration. The remaining OCR was considered as non-mitochondrial respiration. To calculate the mitochondrial respiration, non-mitochondrial OCR was subtracted from the total OCR. Data were normalized to cell number in the wells and presented as pmol/min/10 000 cells. Recombinant mouse IGF2 (R&D Systems, MN, USA), 5-40 ng/mL was supplemented to the culture medium for 24 hours before measurement.

3 | RESULTS

3.1 | Efficient deletion of *Zbed6* and its binding site in *Igf2*

In order to explore to which extent phenotypic changes associated with altered expression of ZBED6 is due to its interaction with the *Igf2* locus, we established two genetically engineered C2C12 cell lines, one with complete *Zbed6* inactivation and the other with a deletion of the ZBED6 binding site in the first intron of the *Igf2* gene (chr7:142,664,244-142,664,249, mmu10) (Figure 1A,B). The CRISPR/Cas9 method was used to delete almost the entire coding sequence (2.5 kb out of 2.9 kb) of *Zbed6* in C2C12 cells (Figure 1A). We genotyped 150 clones using multiplex PCR (Figure 1C) and found that 10% of the clones were untargeted, while 90% were targeted with at least one gRNA. Of these clones, 22%

showed a frameshift in one allele, 74% showed a 2.5 kb deletion of ZBED6 in a single allele and 4% of the clones showed a 2.5 kb deletion in both alleles.

The ZBED6 binding motif 5′-GGCTCG-3′ in *Igf2* intron 1 was targeted using a gRNA that cleaves between the C and T nucleotides (Figure 1B). PCR screening of C2C12 clones revealed several clones with deletions at this site, ranging in size from 4 to 120 nucleotides. One of the clones showed a four-nucleotide deletion (GGCT) of the binding motif in both alleles. We named this clone $Igf2^{\Delta GGCT}$ and used it for all downstream analysis together with the $Zbed6^{-/-}$ clones; a second clone ($Igf2^{\Delta 120bp}$) was used to confirm the effect on cell growth (see below). The expression of the ZBED6 protein in the $Zbed6^{-/-}$ and $Igf2^{\Delta GGCT}$ clones was evaluated by immunoblot analysis, which revealed complete ablation of ZBED6 expression in $Zbed6^{-/-}$ clones and normal expression in $Igf2^{\Delta GGCT}$ cells in comparison to WT C2C12 cells (Figure 1D).

3.2 | Both $Zbed6^{-/-}$ and $Igf2^{\Delta GGCT}$ myoblasts exhibit faster cell growth and massive upregulation of *Igf2* expression

The real-time measurement of growth rate showed that both $Zbed6^{-/-}$ and $Igf2^{\Delta GGCT}$/$Igf2^{\Delta 120bp}$ clones grow faster than the WT (Cas9) cells (Figure 1E,F); the WT (Cas9) cells here refer to WT cells treated with CRISPR/Cas9 reagents without gRNA and kept at similar selection conditions as the targeted cells. In order to explore the effect of this condition on cell growth, we measured the growth rate of WT (Cas9) vs the WT C2C12 cells at early (P5), middle (P12), and late (P20) cell passages. The WT (Cas9) had similar growth rate as the WT C2C12 cells at early and middle passage, while the late passage C2C12 cells grew slower (Figure 1G).

Expression analysis using quantitative reverse transcriptase PCR (RT-qPCR) revealed a more than 30-fold upregulation of *Igf2* mRNA when ZBED6 was deleted or its binding site in *Igf2* was disrupted (Figure 1H). To verify that the increased expression of *Igf2* in $Zbed6^{-/-}$ and $Igf2^{\Delta GGCT}$ cells, indeed, was caused by the loss of ZBED6 or its binding site, we generated and validated an expression construct that produces a ZBED6-GFP fusion protein (Figure 1I,J). We reintroduced ZBED6 into the $Zbed6^{-/-}$ and $Igf2^{\Delta GGCT}$ clones by transient overexpression of ZBED6-GFP (ZBED6-OE). The GFP construct was used as control. qPCR analysis confirmed an efficient overexpression of *Zbed6* in WT, $Zbed6^{-/-}$, and $Igf2^{\Delta GGCT}$ cells (Figure 1I). The overexpression of *Zbed6* in WT cells resulted in a significant 60% downregulation of *Igf2* mRNA. Interestingly, reintroduction of ZBED6-GFP in $Zbed6^{-/-}$ clones significantly downregulated the elevated expression of *Igf2*, while no changes were observed when ZBED6-GFP was overexpressed in $Igf2^{\Delta GGCT}$ clones (Figure 1H). These results imply that ZBED6 represses *Igf2* expression exclusively through interaction with its binding site in *Igf2* intron 1.

3.3 | $Zbed6^{-/-}$ and $Igf2^{\Delta GGCT}$ myoblasts develop myotube hypertrophy with improved contractile properties after differentiation

The differentiation profile of $Zbed6^{-/-}$ and $Igf2^{\Delta GGCT}$ myoblasts was assessed by time-lapse microscopy (Supporting Information Video) and immunofluorescence staining of myotubes using myogenin and myosin heavy chain (MyHC) antibodies (Figure 2A). The differentiation of $Zbed6^{-/-}$ and $Igf2^{\Delta GGCT}$ myoblasts resulted in formation of hypertrophic myotubes post 4 days of differentiation induction (Figure 2A), with significant increase in the differentiation index and myotube diameter in $Zbed6^{-/-}$ and $Igf2^{\Delta GGCT}$ myotubes in comparison to WT cells (Figure 2B,C). The length of the hypertrophic myotubes was significantly shorter than the WT myotubes (Figure 2D). This was associated with increased MyHC and myogenin expression in $Zbed6^{-/-}$ and $Igf2^{\Delta GGCT}$ myotubes (Figure 2E,F).

3.4 | Quantitative SILAC proteomic and transcriptomic analyses of $Zbed6^{-/-}$ and $Igf2^{\Delta GGCT}$ myoblasts

To determine the possible transcriptional targets of ZBED6 during myogenesis, we performed both transcriptomic and mass spectrometry (MS)-based quantitative proteomic analyses of $Zbed6^{-/-}$, $Igf2^{\Delta GGCT}$, and WT myoblasts. Differentially regulated genes/proteins and pathways were analyzed with a special focus on genes that showed differential expression in both $Zbed6^{-/-}$ and $Igf2^{\Delta GGCT}$ myoblasts in order to explore to which extent the observed changes in gene expression in $Zbed6^{-/-}$ clones are secondary effects due to increased IGF2 expression.

The SILAC-MS technique was used to quantitate the changes in the total proteome of the mutant myoblasts. Quantitation analysis using MaxQuant identified around 4000 proteins in each cell line with at least two unique peptides detected in each replicate. The DE analysis of SILAC data showed 312 and 855 DE proteins in $Zbed6^{-/-}$ medium and lysate fractions, respectively, and 220 and 350 DE proteins in $Igf2^{\Delta GGCT}$ medium and lysate fractions, respectively ($P < .05$, after Benjamini-Hochberg correction for multiple testing), (Figure S1, Table S1). The transcriptome analysis of $Zbed6^{-/-}$, $Igf2^{\Delta GGCT}$, and WT myoblasts identified around 12 000 expressed genes with at least one read count per million (cpm). DE analysis of transcriptome data revealed ~3000 DE genes in $Zbed6^{-/-}$ and ~2500 in $Igf2^{\Delta GGCT}$ myoblasts

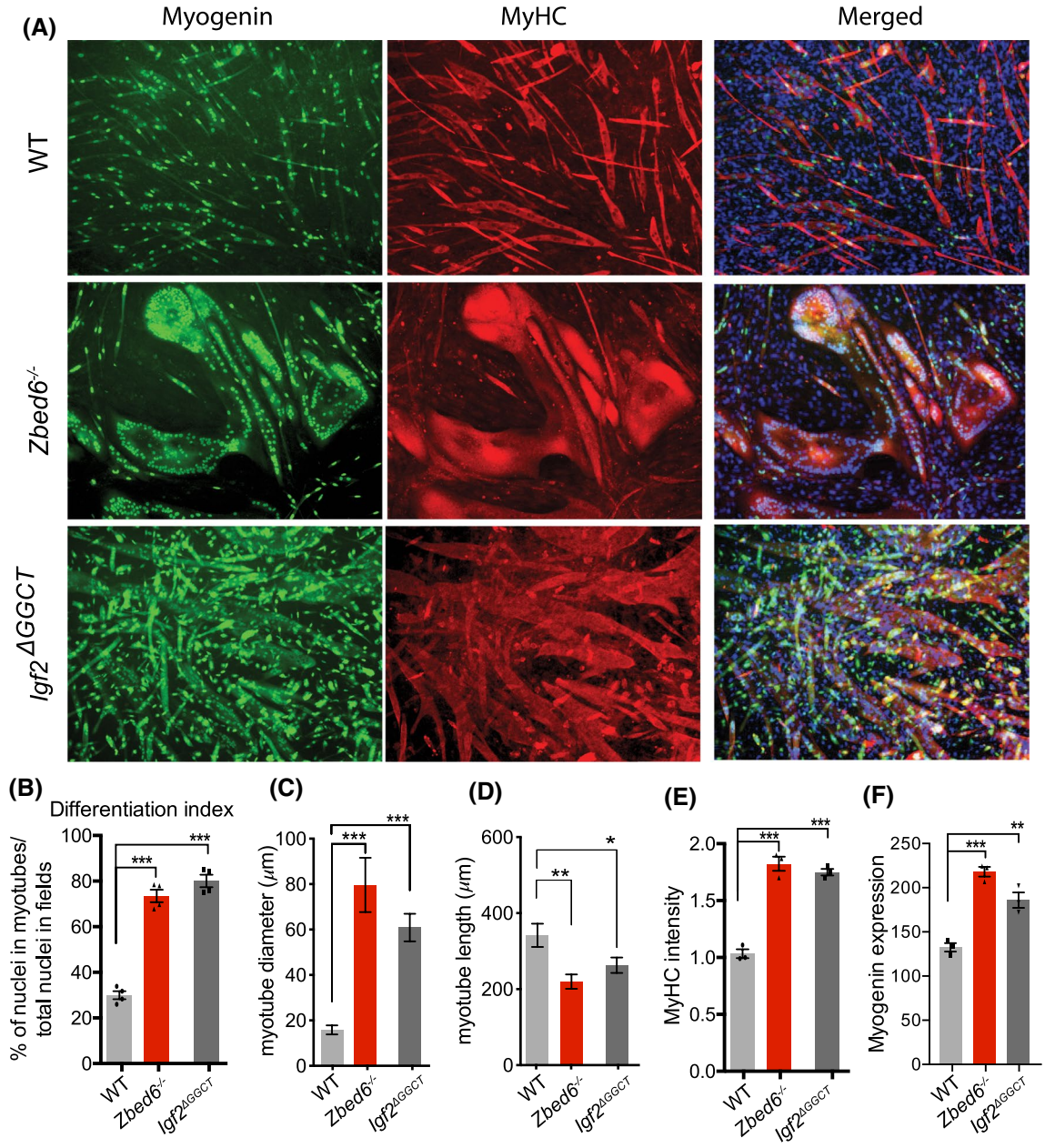

FIGURE 2 *Zbed6*$^{-/-}$ and *Igf2*$^{\Delta GGCT}$ myoblasts develop hypertrophic myotubes. A, Immunofluorescence staining of 4 days differentiated WT, *Zbed6*$^{-/-}$ and *Igf2*$^{\Delta GGCT}$ myotubes using anti-myogenin antibody (green), anti-myosin-heavy chain (MyHC) antibody (red),and DAPI (blue). B, Differentiation index of WT, *Zbed6*$^{-/-}$, and *Igf2*$^{\Delta GGCT}$ myotubes, calculated as the percentage of nuclei in myotubes to the total number of nuclei in the same field.[40] C and D, Diameter and length of myotubes. E, The relative intensity of MyHC staining in the differentiated myotubes. F, qPCR analysis of *Myogenin* expression in myotubes, the graph presents the relative expression to WT myoblast (mean ± SEM), $^{**}P < .01$, $^{***}P < .001$, Student's *t* test

(Table S2). We integrated the SILAC and RNA-seq data in order to explore the correlation between changes in mRNA and protein expression, to gain further understanding of how the ZBED6-*Igf2* axis affects myoblasts. We detected 381 and 196 genes to be DE in both SILAC and RNA-seq in *Zbed6*$^{-/-}$ and *Igf2*$^{\Delta GGCT}$ myoblasts, respectively. Moreover, we found a significant positive correlation between DE genes and proteins in *Zbed6*$^{-/-}$ ($r = .49$) and *Igf2*$^{\Delta GGCT}$ ($r = .55$) myoblasts (Figure 3A). Strikingly, the dramatic upregulation of *Igf2* was detected in both *Zbed6*$^{-/-}$ and *Igf2*$^{\Delta GGCT}$ myoblasts at both the transcriptome and proteome level (Figure 3A).

In order to distinguish between the DE genes caused by ZBED6 inactivation and those that are secondary due to *Igf2* upregulation, we calculated the overlap between DE genes and proteins in both *Zbed6*$^{-/-}$ and *Igf2*$^{\Delta GGCT}$ myoblasts. This analysis showed 56 shared DE proteins in *Zbed6*$^{-/-}$ and *Igf2*$^{\Delta GGCT}$ cells, and 325 DE proteins unique to *Zbed6*$^{-/-}$ myoblasts, while 140 was unique to *Igf2*$^{\Delta GGCT}$ cells (Figure 3B, left). KEGG

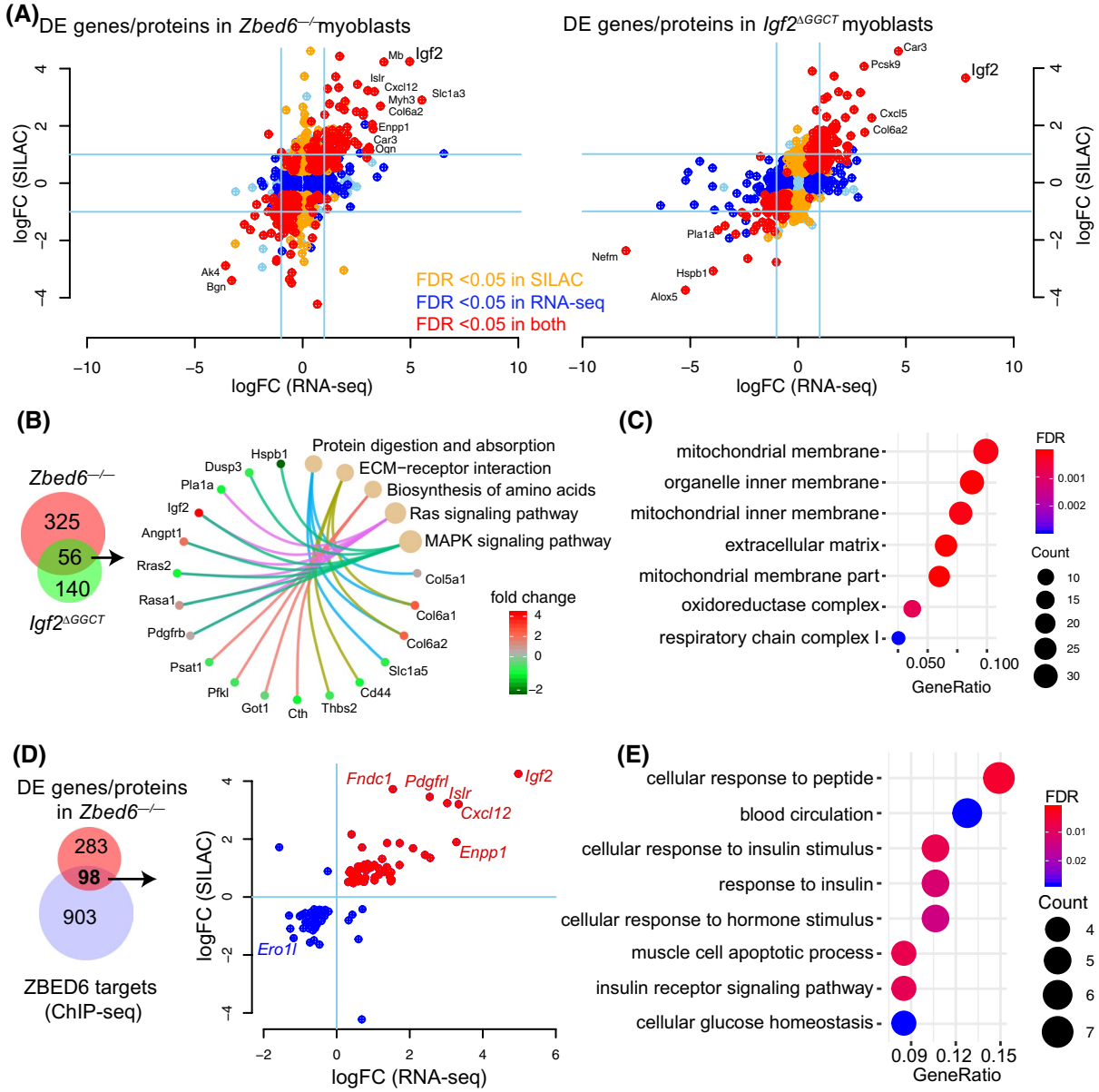

FIGURE 3 SILAC proteomic and transcriptome analyses of *Zbed6*$^{-/-}$ and *Igf2*$^{\Delta GGCT}$ myoblasts. A, Expression of identified proteins and genes by SILAC and RNA-seq data in *Zbed6*$^{-/-}$ (left) and *Igf2*$^{\Delta GGCT}$ (right) myoblasts. The values are presented as log fold change (logFC) to WT cells and colored based on the FDR < 0.05 values. B, Intersection of DE proteins in both *Zbed6*$^{-/-}$ and *Igf2*$^{\Delta GGCT}$ myoblasts (left), KEGG pathway analysis of the shared 56 DE proteins (right). C, GO analysis of the 325 DE proteins in *Zbed6*$^{-/-}$ myoblasts. GeneRatio indicates the number of genes found in each term as a proportion of the total number of examined genes. D, Intersection of DE proteins in *Zbed6*$^{-/-}$ myoblasts and putative ZBED6 targets that are expressed in C2C12 cells and detected by SILAC and RNA-seq (left), the fold changes of genes/proteins with ZBED6 binding sites (right). E, GO analysis of upregulated genes/proteins in *Zbed6*$^{-/-}$ myoblasts with ZBED6 binding sites

pathway analysis of those 56 shared DE proteins revealed a significant enrichment of proteins involved in extra cellular matrix (ECM)−receptor interaction, and the MAPK and RAS signaling pathways (Figure 3B, right). Interestingly, the cellular component analysis of DE proteins unique to *Zbed6*$^{-/-}$ myoblasts showed a significant enrichment for mitochondrial membrane proteins (Figure 3C), while a similar analysis for the 56 shared DE proteins and the DE proteins unique to *Igf2*$^{\Delta GGCT}$ myoblasts showed an enrichment for extracellular matrix proteins, and not for mitochondrial terms (Figure S2).

Our previous ChIP-seq analysis for ZBED6 identified thousands of putative target genes in C2C12 myoblasts.[1,4] Here, we combined the SILAC, RNA-seq, and ChIP-seq data to find out functional targets for ZBED6. The previously described ChIP-seq peaks in C2C12 cells were associated with about 3000 genes, that is, about 15% of the genes in the mouse genome. As many as 1001 of the about 4000 proteins (25%) detected in the SILAC analysis corresponded to a gene associated with a ZBED6 ChIP-seq peak. This highly significant overrepresentation ($P < .001$) is consistent with the notion

that ZBED6 binds open chromatin.[4] Since 25% of the proteins detected by SILAC corresponded to a gene associated with a ChIP-seq peak it is expected that 25% (95) of the 381 genes detected as DE both at the mRNA and protein level due to chance only. We found 98 genes in our data (Figure 3D, left). This implies that we cannot draw any firm conclusion on true ZBED6 targets in mouse C2C12 cells, other than the well-established *Igf2* locus, based on these data. In fact, *Igf2* is the gene showing the most striking DE gene between WT and *Zbed6*$^{-/-}$ cells (Figure 3D, right). However, five other genes, highlighted in Figure 3D, showed a striking upregulated expression after silencing of the ZBED6 repressor, suggesting that they may be functional targets. The gene ontology (GO) analysis of the transcripts with significant upregulation in *Zbed6*$^{-/-}$ myoblasts and associated with ChIP-seq peaks showed a significant enrichment for proteins involved in cellular response to insulin stimulus (Figure 3E). These genes include *Insulin-Like Growth Factor 1 Receptor* (*Igf1r*), *Phosphoinositide-3-Kinase Regulatory Subunit 1 (Pik3r1)*, and *Ectonucleotide pyrophosphatase phosphodiesterase 1* (*ENPP1*), a negative modulator of insulin receptor (IR) activation.

3.5 | ZBED6 modulates transcriptional regulation of differentiated myotubes partially through IGF2 signaling

To investigate the possible role of the ZBED6-*Igf2* axis on transcriptional regulation during myogenesis, we performed transcriptome analyses of *Zbed6*$^{-/-}$, *Igf2*$^{\Delta GGCT}$ and WT cells after differentiation into myotubes. First, we analyzed the DE genes in WT myoblasts vs myotubes to explore the overall transcriptional changes during myotube formation. The counting of aligned reads using the STAR tool[21] identified ~12 000 expressed genes in myoblasts with at least one read count per million (cpm) (Figure S3A). The expression of ~3900 genes was found to be changed significantly, with 2200 upregulated and 1700 downregulated genes after differentiation into myotubes ($P < .05$, after Benjamini-Hochberg correction for multiple testing), (Figure S3B). GO analysis of upregulated genes revealed a significant enrichment of cell adhesion, muscle proteins and muscle contraction genes, while the downregulated genes were enriched for cell cycle and mitotic nuclear division categories (Figure S3C).

Transcriptome analysis comparing WT and *Zbed6*$^{-/-}$ cells after differentiation identified 2673 DE genes (log fold change > 0.5; $P < .05$, after Benjamini-Hochberg correction for multiple testing), with 1243 upregulated and 1430 downregulated genes. Furthermore, 2630 genes showed a significant differential expression in the comparison of *Igf2*$^{\Delta GGCT}$ and WT cells after differentiation, with 1278 upregulated and 1352 downregulated in mutant cells (Table S4). The dissection of the DE genes based on the direction of the change revealed a highly significant (Chi-square test, $P < .001$) 30% overlap between DE genes in *Zbed6*$^{-/-}$ and *Igf2*$^{\Delta GGCT}$ myotubes (Figure 4A).

The expression of *Igf2* is known to be upregulated during myoblast differentiation.[7] In this study, we detected the same pattern as *Igf2* was upregulated 100-fold after differentiation of WT cells (Figure 4B). Furthermore, the *Igf2* mRNA expression was upregulated 500-fold in *Zbed6*$^{-/-}$ and *Igf2*$^{\Delta GGCT}$ myotubes in comparison to WT myoblast and six-fold in comparison to WT myotubes (Figure 4B). Interestingly, this upregulation of *Igf2* expression was accompanied with a significant but modest increase in the expression of the endogenous *Zbed6* mRNA (Figure 4C), which indicates a positive correlation between *Igf2* and *Zbed6* expression.

The GO analysis of the upregulated genes in both *Zbed6*$^{-/-}$ and *Igf2*$^{\Delta GGCT}$ myotubes exhibited a striking enrichment of muscle-specific genes (Figure 4D, left). This included genes for myosin heavy and light chains (*Myl1, Myl2, Myh1, Myh2, Myh7,* and *Myh8*), troponins (*Tnnt1, Tnnt3, Tnnc1,* and *Tnni2*), myomesins (*Myom1* and *Myom2*), alpha actinin (*Actn2 and Actn3*), leiomodin (*Lmod2* and *Lmod3*), titin (*Ttn*) and myoglobin (*Mb*). In contrast, genes involved in cell division and cell cycle regulation such as cyclins (*Ccnb1*, *Ccna2,* and *Ccnb2*), were enriched among downregulated genes in both *Zbed6*$^{-/-}$ and *Igf2*$^{\Delta GGCT}$ myotubes (Figure 4D, right). The expression of genes belonging to these GO categories is presented as logCPM values in myoblast and myotubes (Figure 4E,F). The results demonstrate a remarkable shift in their expression before and after differentiation, and how these differences are enhanced in *Zbed6*$^{-/-}$ and *Igf2*$^{\Delta GGCT}$ myotubes.

3.6 | ZBED6 overexpression impairs myoblast differentiation

The role of ZBED6 in myogenesis was further investigated by overexpressing ZBED6 (ZBED6-OE) in C2C12 myoblasts and then induce differentiation. Immunofluorescence staining against myogenin and MyHC revealed poor differentiation of ZBED6-OE myoblasts, with a marked reduction in cells expressing myogenin and myosin (Figure 5A). This observation was in stark contrast to the myotube hypertrophy observed in *Zbed6*$^{-/-}$ C2C12 cells after differentiation (Figure 2A). We performed RNA-seq analysis of ZBED6-OE and control cells after 72 hours of differentiation. The bioinformatic analysis of differentiated myoblasts revealed 1560 downregulated genes and 1157 upregulated genes (log fold change > 0.5; $P < .05$, after Benjamini-Hochberg correction for multiple testing) in ZBED6-OE vs control cells (Figure S4). The most affected genes in response to ZBED6-OE included downregulation of *Igf2,* myogenin (*Myog*), and myosin heavy chain 3 (*Myh3*)

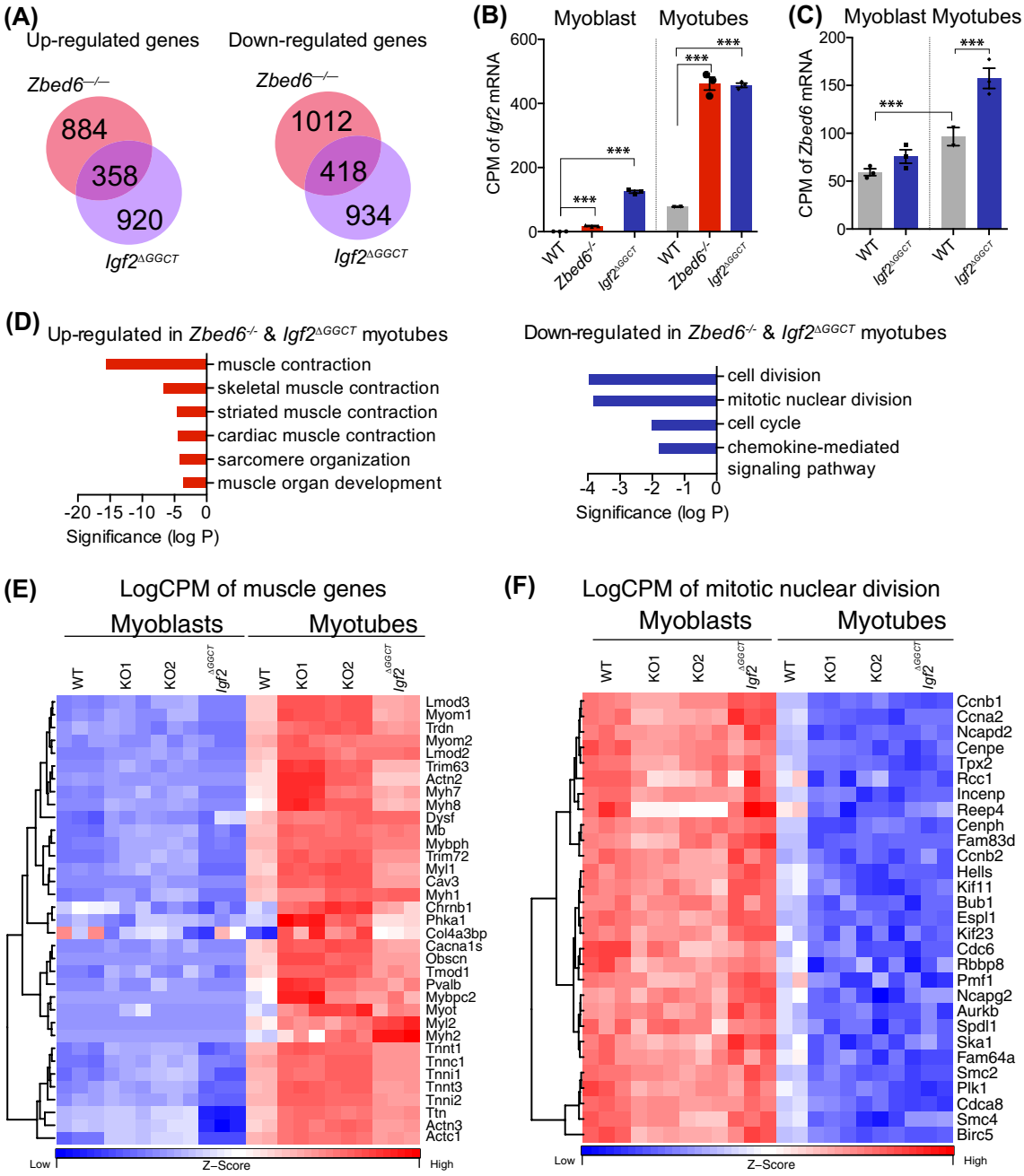

FIGURE 4 Transcriptome analysis of *Zbed6*$^{-/-}$ and *Igf2*$^{\Delta GGCT}$ myotubes. A, Intersection of upregulated and downregulated DE genes in *Zbed6*$^{-/-}$ myotubes (red) vs *Igf2*$^{\Delta GGCT}$ myotubes (blue). B and C, The expression analysis of *Igf2* (B) and *Zbed6* (C) mRNA in WT, *Zbed6*$^{-/-}$, and *Igf2*$^{\Delta GGCT}$ myoblasts and myotubes as counts per million (CPM). D, GO analysis of upregulated (left) and downregulated (right) DE genes in both *Zbed6*$^{-/-}$ and *Igf2*$^{\Delta GGCT}$ myotubes. Bars show multiple testing corrected *P*-value for enriched GO categories. E, Heatmap of muscle-specific genes that were found in muscle contraction GO categories. Expression values are presented as logCPM and color-scaled from blue (low-expression) to red (high-expression). Each column represents an individual sample of *Zbed6*$^{-/-}$ (KO1 and KO2), *Igf2*$^{\Delta GGCT}$, and WT groups. F, Heatmap of genes that were found in cell cycle and mitotic nuclear division GO categories

(Figure 5B, Figure S4). The GO analysis of downregulated genes showed a significant enrichment of muscle-specific genes, while the upregulated genes were primarily related to cell cycle regulation and cell division (Table 1), thus the opposite trend compared with *Zbed6*$^{-/-}$ cells. As many as 463 genes were significantly downregulated in differentiated ZBED6-OE myoblasts and significantly upregulated in *Zbed6*$^{-/-}$ myotubes (Figure 5C). These represent about 40% of the upregulated genes in *Zbed6*$^{-/-}$ myotubes. We examined these genes and the corresponding pathways in more detail. The GO analysis revealed a striking enrichment in muscle-specific categories (Table S5). Among the enriched KEGG pathways, we found cardiac muscle contraction, hypertrophic cardiomyopathy (HCM), and calcium, insulin and

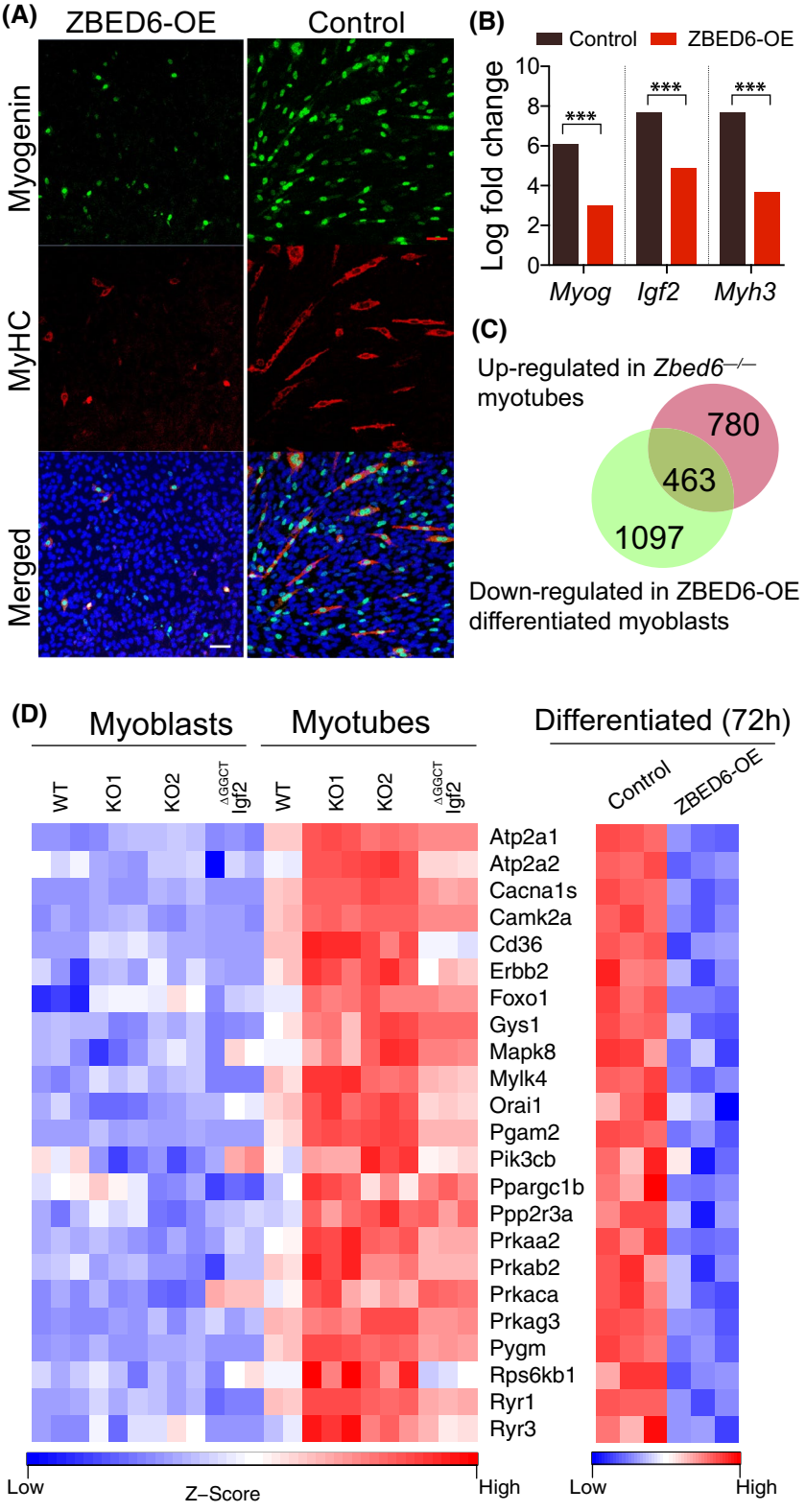

FIGURE 5 Overexpression of ZBED6 impairs myotube differentiation. A, Immunofluorescence staining of myogenin and MyHC in 72 hours differentiated myoblasts transiently overexpressing ZBED6 (ZBED6-OE). (Scale bar: 50 μm). B, Log fold change in the expression of *Myog*, *Igf2,* and *Myh3* mRNA in control and ZBED6-OE differentiated myoblasts in comparison to un-differentiated control myoblasts (***$FDR < 0.001$). C, Intersection of upregulated DE genes in *Zbed6*$^{-/-}$ myotubes (red) vs downregulated DE genes in ZBED6-OE differentiated myoblasts (green). D, Heatmap of genes found in the AMPK and insulin signaling pathways

AMPK signaling (Table S5). We examined the genes present in the AMPK and insulin signaling pathways and compared their expression in *Zbed6*$^{-/-}$, *Igf2*$^{\Delta GGCT}$, and *ZBED6-OE* cells after differentiation. Interestingly, the key components of these pathways were found to be upregulated in *Igf2*$^{\Delta GGCT}$ myotubes as well (Figure 5D). For instance, the expression of phosphatidylinositol-4,5-bisphosphate 3-kinase catalytic subunit beta (*Pik3cb*), glycogen synthase 1 (*Gys1*) and AMP-activated protein kinase alpha2 (*Prkaa2*), beta2 (*Prkab2*), and gamma3 (*Prkag3*) subunits were found to be upregulated in *Zbed6*$^{-/-}$ and *Igf2*$^{\Delta GGCT}$ myotubes, and downregulated in ZBED6-OE differentiated cells (Figure 5D). Activation of

TABLE 1 Gene ontology analysis of upregulated and downregulated differentially expressed genes in ZBED6-overexpressing vs control (GFP) myoblasts before and after differentiation

Term	Count	FDR
Downregulated		
Muscle contraction	28	2.5×10^{-11}
Cell adhesion	75	1.2×10^{-9}
Multicellular organism development	129	6.6×10^{-9}
Cardiac muscle contraction	24	3.1×10^{-8}
Skeletal muscle contraction	19	4.3×10^{-8}
Upregulated		
Cell cycle	127	4.7×10^{-25}
Mitotic nuclear division	81	9.3×10^{-24}
Cell division	92	1.4×10^{-22}
DNA replication	39	7.4×10^{-10}
Chromosome segregation	30	1.1×10^{-8}

the PI3K pathway and its downstream targets plays a central role in myogenesis. Interestingly, *Prkaa2*, *Prkab2,* and *Prkag3*, all upregulated in *Zbed6*$^{-/-}$ and *Igf2*$^{\Delta GGCT}$ myotubes, encode the AMPK α2, β2, and γ3 subunits. These subunits form a specific isoform of AMPK that shows tissue-specific expression in white skeletal muscle.[26] The results imply that the interaction between ZBED6-*Igf2* has an essential role in muscle development and influences muscle metabolism.

3.7 | Overexpression of ZBED6 in non-differentiated C2C12 cells results in reduced cell viability and cell cycle arrest

Since deletion of ZBED6 promotes cell proliferation and myogenesis, we investigated whether the overexpression of ZBED6 causes the opposite effect. Unfortunately, we did not succeed in our attempts to establish a stable myoblast cell line overexpressing ZBED6, suggesting that overexpression may be lethal in C2C12 cells, which is consistent with the results of a previous study.[27] Therefore, we measured cell viability after transient overexpression of ZBED6 (ZBED6-OE) in C2C12 cells. We found a significant reduction in cell viability in ZBED6-OE cells in comparison to control cells (Figure S5). The cell apoptosis analysis using flow cytometry revealed a significant reduction in the number of live cells in ZBED6-OE (Figure 6A). Moreover, cell cycle analysis using flow cytometry displayed a significant difference in the proportion of cells in different cell cycle phases, in which 82% of ZBED6-OE cells appeared to be in the G0/G1 phase and 10% in the S-phase, whereas the corresponding proportions in control cells were 58% and 35%, respectively (Figure 6B). These phenotypic changes in ZBED6-OE myoblasts were in complete agreement with the RNA-seq analysis that revealed a significant enrichment of genes involved in cell cycle and cell division processes among the downregulated genes after ZBED6-OE in proliferating myoblasts (Table 2). Out of 98 downregulated cell cycle-related genes, 21 were previously identified as putative direct targets of ZBED6[1,4] (Figure 6C). Some of the putative direct targets with essential role in cell cycle regulation were validated by qPCR (Figure S6). These included the genes for E2f1 and E2f2, members of the E2f family that has an essential role in regulating cell proliferation and controls the transition from G1 to S phase.[28] There was a striking upregulation of genes involved in immune defense after ZBED6-OE in proliferating myoblasts (Table 2). These results suggest that ZBED6 inhibits proliferation and promotes immune defense in C2C12 cells.

3.8 | Changes in mitochondrial activity in response to altered ZBED6 expression in myoblasts

The strong correlation between mitochondrial biogenesis and aerobic metabolism, on the one hand, and mesenchymal stem cell differentiation, on the other hand, is well established.[29-31] The marked increase in mitochondrial activity that occurs during mesenchymal differentiation is driven by the transcription factor PGC-1α, and IGF2 has been suggested to participate in this process.[32] Moreover, RNA-seq and SILAC proteomic analyses showed a significant enrichment for mitochondrial membrane proteins among DE proteins in *Zbed6*$^{-/-}$ myoblasts (Figure 3C). These observations encouraged us to look closer at mitochondrial activities in response to ZBED6-overexpression or ablation. Flow cytometry analysis of MitoTracker Red intensity, a dye that labels active mitochondria in living cells, indicated a significant reduction in mitochondrial mass in ZBED6-OE cells and an increase in mitochondria in *Zbed6*$^{-/-}$ cells, while no change was observed in *Igf2*$^{\Delta GGCT}$ cells (Figure 6D,E). As MitoTracker Red labeling only gives a very crude estimate of mitochondrial mass and activity, we also stained transiently ZBED6-GFP transfected C2C12 cells with JC-1, a probe that gives an estimate of the inner mitochondrial membrane potential. These experiments demonstrated that ZBED6-GFP overexpressing cells displayed lower JC-1 aggregates (red fluorescence) to JC-1 monomers (green fluorescence) ratio (Figure 6F,G), indicating a decreased mitochondrial membrane potential in response to overexpressed ZBED6. Both the MitoTracker and JC-1 experiments are in agreement with the SILAC data, and suggest an inhibitory role of ZBED6 on mitochondrial mass/function. Since both *Zbed6*$^{-/-}$ and *Igf2*$^{\Delta GGCT}$ myoblasts exhibited similar phenotypic characteristics regarding growth and differentiation, we explored another part of

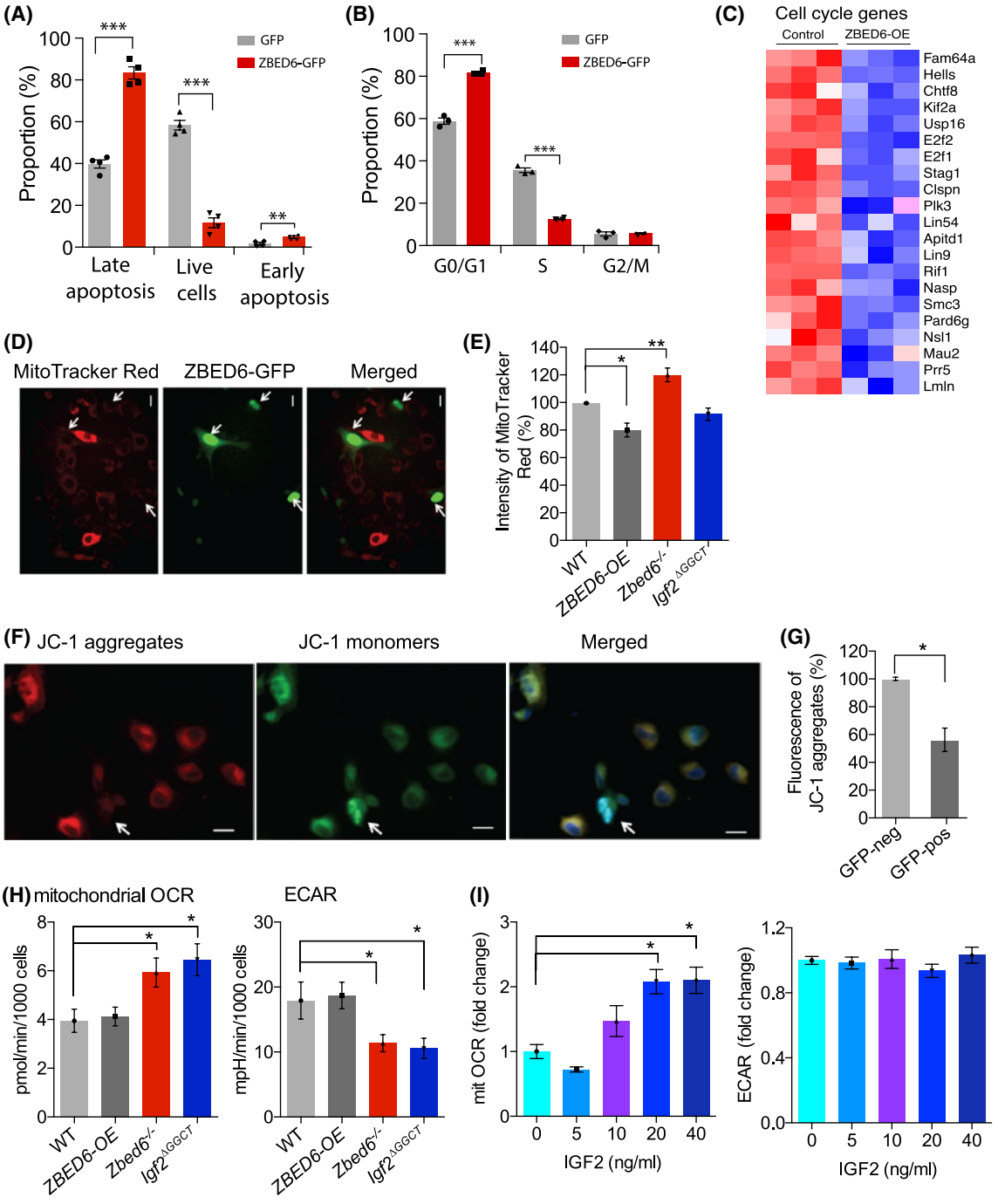

FIGURE 6 Overexpression of ZBED6 leads to reduced cell viability, cell cycle arrest, and reduced mitochondrial activity. A, Cell apoptosis assay of myoblasts overexpressing ZBED6-GFP fusion protein vs the control myoblasts expressing GFP. B, Cell cycle analysis of myoblasts overexpressing ZBED6-GFP fusion protein vs GFP expressing cells. C, The expression of downregulated genes found in cell cycle GO categories and containing the consensus ZBED6 binding motif within 1kb of their TSS.[1,4] D, MitoTracker Red labeling of ZBED6 transient overexpressing (ZBED6-GFP) cells. E, Flow cytometry analysis of the intensity of MitoTracker Red labeling of active mitochondria in WT, ZBED6-overexpression (ZBED6-OE), *Zbed6*$^{-/-}$, and *Igf2*$^{\Delta GGCT}$ cells. F, A representative image of JC-1 aggregates, JC-1 monomer of ZBED6-GFP cells to measure the mitochondrial hyperpolarized membrane potentials. G, Quantitation of the fluorescence intensity of JC-1 aggregates (red) in WT (GFP-neg) and transient ZBED6-OE (GFP-pos) using ImageJ. (Totally 104 WT and 50 ZBED6-OE cells were quantified from three independent experiments.). H, The oxygen consumption rate (OCR) and extracellular acidification rate (ECAR) were determined with the Extracellular Flux Analyzer XFe96 in C2C12 cells (WT, ZBED6-OE, *Zbed6*$^{-/-}$, and *Igf2*$^{\Delta GGCT}$). Results are means ± SEM for five independent observations. (I) OCR and ECAR were determined in C2C12 WT cells supplemented with 5, 10, 20, and 40 ng/ml IGF2 in culture medium. Results were normalized to control condition and are means ± SEM for at least six replicates in each condition. *Denotes $P < .05$ vs WT using one-way ANOVA

TABLE 2 Gene ontology analysis of upregulated and downregulated differentially expressed genes in ZBED6-overexpressing vs control (GFP) proliferating myoblasts

Term	Count	FDR
Downregulated		
mRNA processing	63	3.7×10^{-4}
DNA replication initiation	13	6.3×10^{-4}
Cell cycle	98	1.2×10^{-3}
DNA replication	34	1.6×10^{-3}
Mitotic nuclear division	54	8.0×10^{-3}
Upregulated		
Cellular response to interferon-beta	21	1.5×10^{-9}
Immune system process	61	5.3×10^{-8}
Innate immune response	54	7.7×10^{-7}
Defense response to virus	34	1.7×10^{-6}
Oxidation-reduction process	86	4.8×10^{-3}

mitochondrial function in these cells. We analyzed C2C12 cell mitochondrial oxidation rates (OCR) using the Seahorse technique.[33] The OCR and extracellular acidification rate (ECAR) assay revealed an increased OCR (Figure 6H, left) and reduced ECAR in *Zbed6*$^{-/-}$ and *Igf2*$^{\Delta GGCT}$ myoblasts (Figure 6H, right) compared to WT cells. OCR and ECAR were unaffected in ZBED6-OE cells (Figure 6H). As both *Zbed6*$^{-/-}$ and *Igf2*$^{\Delta GGCT}$ myoblasts show increased *Igf2* expression, we hypothesized that the increase in respiration might be an IGF2 effect. To test this hypothesis, we treated cells with recombinant IGF2 and measured the OCR and ECAR dose-response in C2C12 WT cells. We found a two-fold increase in respiration rates at the higher IGF2 concentrations (20 and 40 ng/mL IGF2) (Figure 6I, left), while no changes were detected in the extracellular acidification rates (Figure 6I, right). Thus, it appears that ZBED6 controls myoblast mitochondrial biogenesis/activity partially via IGF2.

4 | DISCUSSION

This study conclusively demonstrates that the interaction between ZBED6 and its binding site in *Igf2* plays a critical role in regulating the development of myogenic cells. This conclusion is based on (i) MS quantitative proteomics and transcriptomic analyses, (ii) the altered growth rate of myoblasts, (iii) effects on myotube formation and maturation, and (iv) assessment of mitochondrial activities. Interestingly, the disruption of the ZBED6 binding site in *Igf2* was sufficient to obtain very similar phenotypic effects as observed in the *Zbed6* knockout demonstrating that the phenotypic effects caused by *Zbed6* inactivation in myoblast cells are largely mediated through the regulation of *Igf2* expression.

The initial development of skeletal muscle occurs prenatally and involves the proliferation of myoblasts, which then exit the cell cycle and start differentiation to form myotubes.[34,35] It has been reported that the number of myoblasts prenatally greatly influences muscle growth postnatally since the number of muscle fibers is fixed at birth.[36,37] This is of particular interest, since ZBED6 inactivation or disruption of the interaction between ZBED6 and the binding site in *Igf2* promotes the proliferation and growth of myoblasts (Figure 1E,F). The *Zbed6*$^{-/-}$ and *Igf2*$^{\Delta GGCT}$ myoblasts had a ~30-fold upregulation in the *Igf2* mRNA expression. This massive increase in *Igf2* expression was rescued toward the levels found in WT cells when ZBED6 was reintroduced in *Zbed6*$^{-/-}$ myoblasts, while no changes were observed in case of *Igf2*$^{\Delta GGCT}$ myoblasts. Thus, ZBED6 represses *Igf2* expression through the binding site located in *Igf2* intron 1.

Our results on myoblast differentiation revealed that *Zbed6*$^{-/-}$ and *Igf2*$^{\Delta GGCT}$ myoblasts were prone to develop mature, hypertrophic and contractile myotubes, with a striking increase in the expression of well-known markers of muscle differentiation, *Igf2*, myogenin and myosin heavy chain (MyHC). In contrast, overexpression of ZBED6 blocked the differentiation of myoblasts, and the expression of *Igf2*, myogenin and MyHC were greatly downregulated. These phenotypic changes are in agreement with our transcriptome data that revealed a significant ~30% overlap between DE genes in *Zbed6*$^{-/-}$ and *Igf2*$^{\Delta GGCT}$ myotubes (Figure 4A). Gene ontology analysis of the upregulated genes in common between *Zbed6*$^{-/-}$ and *Igf2*$^{\Delta GGCT}$ myotubes demonstrated a significant enrichment of muscle-specific categories, including genes encoding myosin heavy and light chains, troponins, titin, myomesins, alpha actinin, leiomodin, and myoglobin. Interestingly, ~40% of the upregulated DE genes in *Zbed6*$^{-/-}$ myotubes were found to be downregulated in differentiated C2C12 cells after overexpressing ZBED6. The GO analysis of those genes showed an enrichment in muscle-specific categories very similar to what we found among upregulated genes in *Zbed6*$^{-/-}$ myotubes.

Stable Isotope Labeling with Amino acids in Cell culture quantitative proteomic analysis of mutant myoblasts revealed a significant enrichment of mitochondrial membrane proteins exclusively among the DE proteins found in *Zbed6*$^{-/-}$ but not *Igf2*$^{\Delta GGCT}$ myoblast (Figure 3C). This observation was confirmed by the decreased mitochondrial membrane potential in response to ZBED6 overexpression (Figure 6D-G). However, the assessment of mitochondrial respiration rate indicated a positive correlation between oxygen consumption rate and the amount of IGF2 protein in myoblasts. This was concluded by the consistent changes in oxygen consumption in *Zbed6*$^{-/-}$ and *Igf2*$^{\Delta GGCT}$ myoblasts, and after the addition of recombinant IGF2 to the growth medium of wild-type myoblasts. Our findings fit well with what has been reported in literature about the essential role of mitochondrial activities

in proliferation and differentiation of myoblasts. For instance, respiration-deficient human myoblasts were growing slower than control cells, exhibited low ATP synthesis and demonstrated sever deficiency in myotube formation.[38] Furthermore, it has been indicated that the basal mitochondrial respiration rate was increased one-fold and the maximal respiration increased four-fold in differentiated myotubes.[39]

We have previously reported that ZBED6 has ~2500 binding sites all over the genome.[1,4] Here we find that the disruption of only one of these binding sites, located in *Igf2* intron 1, resulted in similar phenotypic changes as observed by complete inactivation of *Zbed6* in C2C12 cells. The results suggest that the regulation of IGF2 expression may be the most important role of ZBED6 in skeletal muscle cells, which is consistent with the initial observation that a mutation of this binding site is causing an altered body composition in pigs selected for meat production[3] and our recent characterization of *Zbed6*$^{-/-}$ and *Igf2* knock-in mice.[8] However, ZBED6 is essentially found in all cell types and throughout development, so it may interact with other important targets in other cells or during other stages of development.

In summary, we have shown that the upregulation of *Igf2* expression obtained either by ZBED6 ablation or the deletion of its binding site in intron one of *Igf2*, has an essential role in modulating the metabolism of myogenic cells and promotes differentiation of myoblast cells partially through increasing respiration rate of the mitochondria. This study provides strong support for the notion that the ZBED6-*Igf2* axis has an essential role for muscle metabolism.

ACKNOWLEDGMENTS

We thank Aris Moustakas for valuable comments on the manuscript. The work was funded by grants from The Knut and Alice Wallenberg Foundation and Swedish Research Council. Sequencing was performed by the SNP&SEQ Technology Platform, supported by Uppsala University and Hospital, SciLifeLab, and Swedish Research Council (80576801 and 70374401). Computer resources were provided by UPPMAX, Uppsala University.

CONFLICT OF INTEREST

The authors declare no conflicts of interest.

AUTHOR CONTRIBUTIONS

L. Andersson and N. Welsh conceived the study; S. Younis was responsible for gene editing and most of the characterization of the different cell lines including RNAseq and bioinformatics analysis; S. Younis, X. Cao, and M. Larsson conducted the SILAC proteomics of the cell lines; R. Naboulsi carried out qPCR validation, cell cycle and apoptosis analysis; X. Wang, E. Sargsyan, P. Bergsten, and N. Welsh were responsible for the characterization of mitochondrial function; S. Younis and L. Andersson wrote the paper with input from other authors. All authors approved the manuscript before submission.

REFERENCES

1. Markljung E, Jiang L, Jaffe JD, et al. ZBED6, a novel transcription factor derived from a domesticated DNA transposon regulates IGF2 expression and muscle growth. *PLoS Biol*. 2009;7:e1000256.
2. Younis S, Kamel W, Falkeborn T, et al. Multiple nuclear-replicating viruses require the stress-induced protein ZC3H11A for efficient growth. *Proc Natl Acad Sci U S A*. 2018;115:E3808-E3816.
3. Van Laere A-S, Nguyen M, Braunschweig M, et al. A regulatory mutation in IGF2 causes a major QTL effect on muscle growth in the pig. *Nature*. 2003;425:832-836.
4. Jiang L, Wallerman O, Younis S, et al. ZBED6 modulates the transcription of myogenic genes in mouse myoblast cells. *PLoS One*. 2014;9:e94187.
5. Akhtar M, Younis S, Wallerman O, Gupta R, Andersson L, Sjöblom T. Transcriptional modulator ZBED6 affects cell cycle and growth of human colorectal cancer cells. *Proc Natl Acad Sci*. 2015;112:7743-7748.
6. Wang X, Jiang L, Wallerman O, et al. ZBED6 negatively regulates insulin production, neuronal differentiation, and cell aggregation in MIN6 cells. *FASEB J*. 2018;33:88-100. https://doi.org/10.1096/fj.201600835R.
7. Florini JR, Magri KA, Ewton DZ, et al. 'Spontaneous' differentiation of skeletal myoblasts is dependent upon autocrine secretion of insulin-like growth factor-II. *J Biol Chem*. 1991;266:15917-15923.
8. Younis S, Schönke M, Massart J, et al. The ZBED6-IGF2 axis has a major effect on growth of skeletal muscle and internal organs in placental mammals. *Proc Natl Acad Sci U S A*. 2018;115:E2048–E2057.
9. Jinek M, Chylinski K, Fonfara I, Hauer M, Doudna JA, Charpentier E. A programmable dual-RNA-guided DNA endonuclease in adaptive bacterial immunity. *Science*. 2012;337:816-821.
10. Ran FA, Hsu PD, Wright J, Agarwala V, Scott DA, Zhang F. Genome engineering using the CRISPR-Cas9 system. *Nat Protoc*. 2013;8:2281-2308.
11. Yaffe D, Saxel O. Serial passaging and differentiation of myogenic cells isolated from dystrophic mouse muscle. *Nature*. 1977;270:725-727.
12. Naito Y, Hino K, Bono H, Ui-Tei K. CRISPRdirect: Software for designing CRISPR/Cas guide RNA with reduced off-target sites. *Bioinformatics*. 2015;31:1120-1123.
13. Stöhr G, Tebbe A. Chapter 8. Quantitative LC-MS of proteins. In: Letzel T, ed. *Protein and Peptide Analysis by LC-MS: Experimental Strategies*. Cambridge, UK: The Royal Society of Chemistry; 2011:104-122.
14. Shevchenko A, Wilm M, Vorm O, Mann M. Mass spectrometric sequencing of proteins from silver-stained polyacrylamide gels. *Anal Chem*. 1996;68:850-858.
15. Cox J, Mann M. MaxQuant enables high peptide identification rates, individualized p.p.b.-range mass accuracies and proteome-wide protein quantification. *Nat Biotechnol*. 2008;26:1367-1372.
16. Tyanova S, Temu T, Cox J. The MaxQuant computational platform for mass spectrometry-based shotgun proteomics. *Nat Protoc*. 2016;11:2301-2319.
17. Huber W, Von Heydebreck A, Sültmann H, Poustka A, Vingron M. Variance stabilization applied to microarray data calibration and to the quantification of differential expression. *Bioinformatics*. 2002;18(suppl_1):S96-S104.

18. Ritchie ME, Phipson B, Wu D, et al. Limma powers differential expression analyses for RNA-sequencing and microarray studies. *Nucleic Acids Res*. 2015;43:e47.
19. Smyth GK. Linear models and empirical bayes methods for assessing differential expression in microarray experiments. *Stat Appl Genet Mol Biol*. 2004;3:1-25.
20. Benjamini Y, Hochberg Y. Controlling the false discovery rate: a practical and powerful approach to multiple testing. *J R Stat Soc Ser B*. 1995;57:289-300.
21. Dobin A, Davis CA, Schlesinger F, et al. STAR: Ultrafast universal RNA-seq aligner. *Bioinformatics*. 2013;29:15-21.
22. Anders S, Pyl PT, Huber W. HTSeq-A Python framework to work with high-throughput sequencing data. *Bioinformatics*. 2015;31:166-169.
23. Robinson MD, McCarthy DJ, Smyth GK. edgeR: A Bioconductor package for differential expression analysis of digital gene expression data. *Bioinformatics*. 2009;26:139-140.
24. Robinson MD, Oshlack A. A scaling normalization method for differential expression analysis of RNA-seq data. *Genome Biol*. 2010;11:R25.
25. Huang DW, Sherman BT, Lempicki RA. Systematic and integrative analysis of large gene lists using DAVID bioinformatics resources. *Nat Protoc*. 2008;4:44-57.
26. Barnes BR, Marklund S, Steiler TL, et al. The 5′-AMP-activated protein kinase γ3 isoform has a key role in carbohydrate and lipid metabolism in glycolytic skeletal muscle. *J Biol Chem*. 2004;279:38441-38447.
27. Butter F, Kappei D, Buchholz F, Vermeulen M, Mann M. A domesticated transposon mediates the effects of a single-nucleotide polymorphism responsible for enhanced muscle growth. *EMBO Rep*. 2010;11:305-311.
28. Wu L, Timmers C, Maiti B, et al. The E2F1–3 transcription factors are essential for cellular proliferation. *Nature*. 2001;414:457-462.
29. Duguez S, Sabido O, Freyssenet D. Mitochondrial-dependent regulation of myoblast proliferation. *Exp Cell Res*. 2004;299:27-35.
30. Hsu Y-C, Wu Y-T, Yu T-H, Wei Y-H. Mitochondria in mesenchymal stem cell biology and cell therapy: from cellular differentiation to mitochondrial transfer. *Semin Cell Dev Biol*. 2016;52:119-131.
31. Antico Arciuch VG, Elguero ME, Poderoso JJ, Carreras MC. Mitochondrial regulation of cell cycle and proliferation. *Antioxid Redox Signal*. 2012;16:1150-1180.
32. Lee KY, Singh MK, Ussar S, et al. Tbx15 controls skeletal muscle fibre-type determination and muscle metabolism. *Nat Commun*. 2015;6:8054.
33. Malmgren S, Nicholls DG, Taneera J, et al. Tight coupling between glucose and mitochondrial metabolism in clonal β-cells is required for robust insulin secretion. *J Biol Chem*. 2009;284:32395-32404.
34. Stockdale FE. Myogenic cell lineages. *Dev Biol*. 1992;154:284-298.
35. Dunglison GF, Scotting PJ, Wigmore PM. Rat embryonic myoblasts are restricted to forming primary fibres while later myogenic populations are pluripotent. *Mech Dev*. 1999;87:11-19.
36. Rehfeldt C, Fiedler I, Weikard R, Kanitz E, Ender K. It is possible to increase skeletal muscle fibre number in utero. *Biosci Rep*. 1993;13:213-220.
37. Velloso CP. Regulation of muscle mass by growth hormone and IGF-I. *Br J Pharmacol*. 2008;154:557-568.
38. Herzberg NH, Zwart R, Wolterman RA, et al. Differentiation and proliferation of respiration-deficient human myoblasts. *Biochim Biophys Acta - Mol Basis Dis*. 1993;1181:63-67.
39. Remels AHV, Langen RCJ, Schrauwen P, Schaart G, Schols AMWJ, Gosker HR. Regulation of mitochondrial biogenesis during myogenesis. *Mol Cell Endocrinol*. 2010;315:113-120.
40. Filigheddu N, Gnocchi VF, Coscia M, et al. Ghrelin and des-acyl ghrelin promote differentiation and fusion of C2C12 skeletal muscle cells. *Mol Biol Cell*. 2007;18:986-994.

SUPPORTING INFORMATION

Additional Supporting Information may be found online in the Supporting Information section.

How to cite this article: Younis S, Naboulsi R, Wang X, et al. The importance of the ZBED6-IGF2 axis for metabolic regulation in mouse myoblast cells. *The FASEB Journal*. 2020;34:10250–10266. https://doi.org/10.1096/fj.201901321R